CrystEngComm

Accepted Manuscript

ROYAL SOCIETY OF CHEMISTRY

www.rsc.org/crystengcomm

Ionothermal Synthesis of FeAPO-5 in the Presence of Phosphorous Acid

Eng-Poh Ng,[1*] Jia-Pei Ghoy,[1] Hussein Awala,[2] Aurélie Vicente,[2] Rohana Adnan,[1] Tau Chuan Ling,[3] Svetlana Mintova[2]

[1]School of Chemical Sciences, Universiti Sains Malaysia, 11800 USM, Penang, Malaysia.

[2]Laboratoire Catalyse & Spectrochimie, CNRS-ENSICAEN, Université de Caen, France.

[3]Institute of Biological Sciences, Faculty of Science, University of Malaya, Kuala Lumpur, Malaysia.

*Corresponding author. Tel: +6046534021; e-mail address: epng@usm.my

Abstract

The ionothermal crystallization of FeAPO-5 molecular sieve in the presence of phosphorous acid (H_3PO_3) has been investigated. The use of H_3PO_3 enabled the formation of metastable intermediate phase (FeNKX-2) that transforms into more open-framework crystalline phase (FeAPO-5). The initial raw materials dissolved rapidly in the presence of the [bdmim]Cl polar ionic liquid, and the addition of the Fe^{3+} salt resulted in the crystallization of the FeNKX-2 intermediate. At this stage, the $[bdmim]^+$ cation did not play the role of pore filler for the FeNKX-2 crystalline structure. Consecutive phase transformation from the FeNKX-2 to the FeAPO-5 phase occurred under prolonged ionothermal treatment, and during this stage, the tetrahedral Fe^{3+} species was found not only participating in the construction of the FeAPO-5 framework but also acting as an intermediary electron-transfer medium. The fast crystallization of the FeAPO-5 was explained by the presence of Fe^{3+} as an intermediate electron-transfer medium promoting the fast release of phosphorus nutrient (P^{5+}) from phosphite (P^{3+}) reservoir that was further required for the crystallization of the FeAPO-5 molecular sieve. The use of the ionic liquid as dual solvent and template in combination with H_3PO_3 as an alternative phosphorus source thus opens the possibility to synthesize other microporous materials *via* phase transformation approach.

1. Introduction

The discovery of microporous aluminophosphate (AlPO-*n*) is considered as a breakthrough in zeolite science since it has wide applications as adsorbent,[1,2] catalyst,[3] membrane,[4] sensor,[5] etc.[6,7]. Typically, these zeotype materials are prepared under hydrothermal condition where phosphoric acid (H_3PO_4) is used as a source for phosphorus.

A new route of hydrothermal synthesis of aluminophosphate materials based on phosphorous acid (H_3PO_3) source has also been reported.[8,9] H_3PO_3 is a moderately strong dibasic acid ($pKa_1 = 1.80$, $pKa_2 = 6.15$) with the structural formula $HPO(OH)_2$.[10] The $HPO(OH)_2$ species usually exists in equilibrium with a minor tautomer $P(OH)_3$ where the phosphorus ion exists as P^{3+} state. H_3PO_3 was found to behave differently from H_3PO_4 during the crystallization of aluminophosphite and/or aluminophosphate molecular sieves.[11] In the synthesis process using H_3PO_3 as phosphorus source, the NKX-2 is formed as an aluminophosphite intermediate (180 °C, 6 days) whereas this intermediate phase is not observed in H_3PO_4-containing route.[8] The transformation of microporous aluminophosphates including SAPO-46, AlPO-47, AlPO-41, SAPO-31, AlPO-11, AlPO-5 and AlPO-CJ2 from NKX-2 has been observed but it requires long crystallization time (7–16 days) and high temperature (ca. 200 °C) due to slow release of phosphorus nutrient (P^{5+}) that is required for the crystallization and growth of aluminophosphates.[8,9,12]

Recently, ionothermal synthesis using ionic liquids as solvents and templates has been developed to prepare aluminophosphate molecular sieves.[13-16] The synthesis can be performed either in open or closed vessels. Furthermore, by using ionothermal synthesis method and phosphorous acid (H_3PO_3), the NKX-2 can be obtained within 3 h, which is faster than the hydrothermal approach (6 days).[17]

Isomorphous substitution of transition metals into framework sites of aluminophosphate molecular sieves (MeAPO-*n*) is a useful tool for the modification of the properties of such materials, enabling the study of crystallization process[18,19] and possible applications.[20,21] However, the effect of transition metal on the crystallization process of AlPO-5 *via* ionothermal and H_3PO_3-containing route is still unknown and hence it is worth to be further explored.

In this work, the ionothermal crystallization of FeAPO-5 using phosphorous acid (H_3PO_3) as phosphorus source is reported. The formation process of FeAPO-5 during the ionothermal synthesis was monitored by microscopic and spectroscopic methods. Possible mechanism for the growth of FeAPO-5 crystals was proposed based on the experimental results.

2. Experimental

Synthesis of [bdmim]Cl

[Bdmim]Cl ionic molten salt was prepared by using the modified synthesis procedure from Ref.[22]: 1,2-Dimethylimidazole (45.00 g, 96%, Merck) was dissolved in ethanol (40 mL, 99.7%, QRëc) in a 250 mL round bottom flask. Benzyl chloride (86 mL, 99%, Merck) was then added into the mixture. The resulting solution was refluxed at 100 °C for 6 h. The round bottom flask was cooled down and placed in an ice bath to allow white crystals to precipitate out (Scheme 1). The white crystals were purified and washed with acetone prior to drying in an oven at 100 °C overnight. The pure ionic molten salt was kept in a tight polypropylene bottle and stored in a desiccator. Product yield of 86.4% is obtained. ^{1}H NMR (400 MHz, ppm, D_2O) appears as follows: δ = 2.48 (3H, imidazole N-C(C*H*$_3$)-N), 3.70 (3H, imidazole N-C*H*$_3$), 4.70 (2H, imidazole N-C*H*$_2$-C_6H_5), 7.22 (1H, imidazole N-C*H*=CH-N), 7.24 (1H, imidazole N-CH=C*H*-N) and 7.28-7.41 (5H, phenyl). FT-IR (KBr disk) cm^{-1}: 1036 (imidazolium, C-N), 1452 and 1638

(aromatic C=C), 1530 (imidazolium, C=N), 3497 (O–H stretching). Anal. cacld for $C_{12}H_{15}N_2Cl$: C, 64.72%; H, 6.79%; N, 12.58%; Cl, 15.92%; found: C, 65.03%; H, 6.66%; N, 11.55%; Cl, 16.77%.

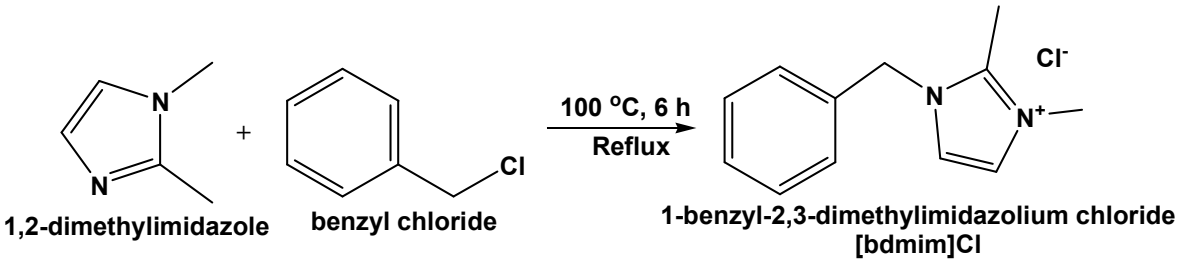

Scheme 1. Synthesis of [bdmim]Cl ionic molten salt.

Ionothermal synthesis of FeAPO-5

The synthesis of FeAPO-5 was carried out in a 50 mL Teflon-lined stainless steel autoclave. Prior to the synthesis, H_3PO_3 (0.421 g, 85%, Sigma-Aldrich) and $FeCl_3.6H_2O$ (0.0178 g, 98%, Merck) were first dissolved in distilled water (0.0743 g). Aluminum isopropoxide (0.416 g, 98%, Sigma-Aldrich) and [bdmim]Cl ionic molten salt (8.89 g) were then introduced into the mixture and the autoclave was sealed prior heating at 170 °C for 10 min. The final gel molar composition for FeAPO-5 was IL : Al : P : Fe : H_2O = 80 : 2 : 6 : 0.13 : 11.5. The reactor vessel was cooled down and the solid product was washed carefully with double distilled water before drying at 80 °C overnight. A similar procedure was also adopted for the solid products after different crystallization time periods (20 min, 1 day, 3 days and 5 days).

Characterization

Powder XRD patterns were recorded on a PANalytical X'Pert PRO diffractometer with Cu K_α radiation (λ = 0.15418 nm, 40 mA, 45 kV, step size of 0.02° and a scan speed of 0.2 °/min). The morphology of the powder samples was analyzed by a Leo Supra 50VP field emission scanning electron microscope (FESEM) operating at 30 kV. The FTIR spectra of samples were obtained using KBr pellet technique in the range of 400–2800 cm^{-1}. The UV-Vis spectra of solids were measured in the spectral range 200–500 nm using a Varian Cary® 100 UV-VIS-NIR spectrophotometer. The ^{27}Al and ^{31}P solid state MAS NMR measurements were conducted on a Bruker Ultrashield 500 spectrometer at MAS frequencies between 5 and 15 kHz. The ^{27}Al and ^{31}P MAS NMR spectra were obtained with 8000 scans by single pulse excitation with $\pi/12$ (0.6 μs) and $\pi/2$ (3 μs) pulses, respectively. Similarly, the ^{13}C solid state CP/MAS NMR measurements were conducted too (spinning speed of 14.5 kHz at magnetic field of 9.4 T with resonance frequency of 104.26 MHz using single pulse mode at 1 ms contact time).

3. Results and discussion

XRD analysis

Fig. 1 shows the XRD patterns of the products. The solid was amorphous after 10 minutes treatment as indicated by the absence of reflections in the X-ray diffractogram. Several diffraction peaks at 2θ = 12.98°, 25.96°, 29.09° and 34.17° appear after 20 min. These peaks are assigned to FeNKX-2, an aluminophosphite intermediate.[8] As compared to NKX-2 aluminophosphite (Fig. 1f), the peaks are slightly right-shifted due to the incorporation of Fe^{3+} into the NKX-2 framework. It is worth to mention here that the incorporation of Fe^{3+} has shortened the crystallization time of NKX-2 to 20 min, which is much faster than those prepared

using ionothermal (170 °C, 5 h) and hydrothermal (195 °C, 6 days) methods reported previously.[8,17] An attempt to use $Fe(NO_3)_3$ instead of $FeCl_3$ as the Fe^{3+} source was also performed in order to study the effect of salt used, and fully crystalline FeNKX-2 was obtained within similar time.

After 1 day of heating, several small peaks at 2θ = 7.46°, 19.77°, 21.15° and 22.47°, which correspond to FeAPO-5 emerge. After extending the crystallization time up to 3 days, the FeAPO-5 phase becomes dominant and fully transformation of FeNKX-2 ferroaluminophosphite intermediate into FeAPO-5 ferroaluminophosphate was achieved within 5 days.

The synthesis was also carried out without adding $FeCl_3$ salt. It was observed that the crystallization time for obtaining the NKX-2 aluminophosphite intermediate was extended to 3 h and this phase was stable with further increase of the heating time, i.e. the AlPO-5 crystalline phase was not detected even after 20 days of ionothermal treatment. An attempt to use H_3PO_4 instead of H_3PO_3 for the synthesis of FeAPO-5 was also made, and no trace of FeNKX-2 was observed for the same gel composition and crystallization conditions.

SEM microscopy study

The crystallization of FeAPO-5 in ionic liquid with H_3PO_3 was followed by SEM analysis. The initial amorphous solid material (10 min) composes of nanoparticles (ca. 120 nm) with irregular shapes (Fig. 2a,b). The nanoparticles tend to agglomerate to form bulk entities with micrometer sizes. The morphology of the bulk solid changes after 20 min; the FeNKX-2 crystals with more pronounced structural features start to form (Fig. 2c,d). As shown in Fig. 2c, the FeNKX-2 crystals (size of ca. 0.6-2.5 μm) show a novel rounded rectangle-like morphology with rough surface, which is different from the hydrothermally and ionothermally synthesized NKX-2

crystals.[8,17] This could be due to the absence of fluoride ion and the use of different ionic liquid ([bdmim]Cl) as a solvent and a template during the ionothermal synthesis.

After 1 day of crystallization, the rounded rectangle-like FeNKX-2 crystals containing FeAPO-5 as minor phase agglomerate with each other and form big spherical particles with a size of ca. 13.8 μm (Fig. 2e,f). With prolongation of the crystallization time up to 3 days, the big spherical particles (ca. 11.5 μm) containing both the FeNKX-2 intermediate and the FeAPO-5 crystalline solids are observed (Fig. 2g,h). As shown, these FeNKX-2 intermediate crystals slowly dissolved in the ionic liquid, and the FeNKX-2 crystals with smooth surface and rectangle-like morphology are appeared and embedded within the big spherical entities (Fig. 2g,h). Furthermore, the FeAPO-5 phase is also observed in the big spherical solid, arranging as stacking layered hexagonal thin flakes. Thus, the change in the morphology of the crystals reveals that phase transformation takes place in the ionic liquid medium, which is in line with the XRD observation (Fig. 1d). The FeNKX-2 phase is completely consumed and pure FeAPO-5 crystals are formed after 5 days of ionothermal treatment (Fig. 2i,j). As can be seen in the micrograph, the resulting crystals are sized about 13.0 μm with stacking layered hexagonal thin flakes growing in rounded hexagonal shaped crystals.

ICP-AES elemental analysis

The elemental compositions of the solids measured by ICP-AES are shown in Table 1. The analysis shows that Fe^{3+} cations participate in the early stage of crystallization process. Initially, 1.53 mol% of Fe is found in the powder solid, and the Fe content keeps increasing with ionothermal synthesis. After 20 min, a P/(Al+Fe) ratio of 1.51 is obtained when the FeNKX-2 solid is formed which corresponds to the P/Al ratio of pure NKX-2 (1.50).[17] The amount of Fe^{3+}

incorporated into the crystalline framework continues to increase where 3.23 mol% of Fe is recorded by the FeNKX-2/FeAPO-5 mixture after 3 days. After 5 days, pure FeAPO-5 with P/(Al+Fe) ratio of 0.99 is measured. The final FeAPO-5 contains 3.39 mol% of Fe, which is higher than the Fe incorporated in the AFI framework using hydrothermal approach (3.0 mol% of Fe).[23]

UV-visible spectroscopy analysis

The incorporation of Fe^{3+} in the solid entities was further investigated with UV-visible spectroscopy. Initially, the amorphous sample with 10 min of heating exhibits two bands at 218 nm and 260 nm (Fig. 3a). The sharp absorption band at 218 nm is attributed to finely dispersed Fe^{3+} in the framework position, whereas the band at 260 nm is due to the ligand to metal charge transfer (LMCT) band of Fe^{3+} in tetrahedral positions.[24] The peaks intensity increases significantly as FeNKX-2 is formed after 20 min (Fig. 3b). Thus, the UV-Vis spectroscopy study reveals that Fe^{3+} participates actively in the construction of the NKX-2 framework. With increasing the heating time, the band at 218 nm slowly disappears. These iron species are gradually converted to tetrahedral framework iron species, where a strong shoulder band at 288 nm slowly appears (Fig. 3e). Furthermore, a weak band at 468 nm also emerges and it can be attributed to the octahedral Fe^{3+} species.[25]

Infrared spectroscopy analysis

Complimentary FTIR spectroscopy study was performed to follow the crystallization kinetic process of the solid. As can be seen in Fig. 4a, only several IR bands are observed in the amorphous sample (10 min) at 2432, 1096, 1017 and 625 cm^{-1} which correspond to P-H

stretching mode of HPO_3^{2-}, symmetrical vibrations of PO_2^-, P–O and TO_4 (T = Al, P or Fe), respectively. After ionothermal heating for 20 min, the solid exhibited the IR spectrum identical to that of pure NKX-2 where the above described bands are slightly shifted to 2469, 1217, 1139, 1036, 588, 549 cm^{-1}.[17] This indicates that the Fe is incorporated in the NKX-2 material. No peak is observed at 1400–1550 cm^{-1} indicating that no $[bdmim]^+$ cation is chemically bound to the amorphous and crystalline FeNKX-2 solids (inset of Fig. 4a,b).

The IR spectra especially at the fingerprint region (1300–400 cm^{-1}) change with further heating. The IR signals at 1426, 1459 and 1544 cm^{-1}, which correspond to $[bdmim]^+$ cation, slowly appear (inset of Fig. 4c-e). Furthermore, the IR bands at 1000–1250 cm^{-1} change slowly and a strong band with a shoulder at 1108 and 1229 cm^{-1} , corresponding to external linkage asymmetrical stretching and internal T–O–T (T = Al, P, Fe) tetrahedral asymmetrical stretching, respectively, are detected after 5 days. Furthermore, the signals at 1036 and 2469 cm^{-1} which are attributed to the P–H stretching and P–H deformation modes of HPO_3^{2-}, respectively, slowly disappear with heating time. Concurrently, four characteristic bands of AFI framework (480, 547, 637 and 740 cm^{-1})[26] start to appear after 3 days, showing that phase transformation to AFI framework structure is taking place, which agrees with the XRD and SEM results. The four characteristic bands for AFI framework are becoming more profound as the solid is further heated to 5 days. The solid exhibits the IR spectrum pattern similar to that of pure AFI phase indicating that fully crystalline FeAPO-5 has been obtained (Fig. 4e).

^{31}P and ^{27}Al MAS NMR spectroscopy analyses

The evolution of the crystalline structure during the amorphous-intermediate-crystal transformation was followed as a function of time by ^{27}Al and ^{31}P MAS NMR spectroscopy. Fig.

5 shows the ^{27}Al and ^{31}P MAS NMR spectra of the solid samples after ionothermal treatment for various times. Initially, two broad signals at –9.7 and 7.3 ppm in the ^{27}Al MAS NMR spectrum are observed which are assigned to the octahedral and pentahedral aluminum species due to $Al(MO)_4(OH_2)_2$ and $Al(MO)_4(OH_2)$ (M = P, Fe), respectively (Fig. 5A(a)).[27] No signals are detected at 1.7 and 61.5 ppm indicating that aluminum isopropoxide has completely dissolved and reacted in ionic liquid after 10 min.[28,29] When the solid is heated for 20 min, the peak at –9.7 ppm is splitted into two peaks at –14.8 and –7.5 ppm (Fig. 5A(b)). The first intense peak at –14.8 ppm is due to the AlO_6 octahedron species, which shares three Al–O corners with three HPO_3^{2-} tetrahedral, and three Al–O with one adjacent AlO_6 octahedron.[8] The second band at –7.5 ppm can be assigned to the $[Al_2(HPO_3)_3]$ species, which are the basic building units of the FeNKX-2 material. These two signals, however, slowly decrease and shift downfield (–14.8 $\rightarrow$ –14.5 ppm and –7.5 $\rightarrow$ –6.2 ppm) with increasing the crystallization time (Fig. 5A(c,d)). This indicates that the matrix suffers from a loss of lattice periodicity due to distorted chemical bonds in Al sites and the presence of AFI crystalline phase. In addition, a new band emerges at 39.9 ppm which is attributed to the tetrahedral Al species in the AFI-type framework.[27] The pentahedral Al signal, on the other hand is shifted from 7.6 ppm to 6.1 ppm. The changes in the ^{27}Al MAS NMR spectra are in a good agreement with the changes observed by the XRD and SEM analyses on the macroscopic level. After 5 days, the peaks in the range of –20 to 0 ppm completely disrupt, producing a broad band at –7.8 ppm. The signal at 38.9 ppm shifts gradually to 38.5 ppm, and is becoming dominant, which suggests that the tetrahedral Al is in a different chemical environment in the fully crystalline FeAPO-5 sample (Fig. 5A(e)). In addition, a significant chemical shift of tetrahedrally coordinated Al is also observed when Fe^{3+} is incorporated in the framework of AlPO-5; the chemical shift of as-synthesized AlPO-5 is 36.0 ppm.[30]

The ^{31}P MAS NMR spectra of the samples are shown in Figure 5B. A broad signal at –4.6 ppm was detected in the sample at the beginning of ionothermal synthesis (10 min) (Fig. 5B(a)). This peak, which is assigned to $P(OH)_2(OM)_2$ (M = Al, Fe), is relatively broad and not well resolved. This indicates a disordered environment around the P site for the sample, which is in agreement with the amorphous character of the XRD pattern (see Fig. 1). Upon ionothermal heating for 20 min, these local environments evolve to become $P(H)(OAl_{Oct})_3$ tetrahedral species where an upfield shift to –13.6 ppm is recorded (Fig. 5B(b)). The signal is sharp due to the symmetry of the tetrahedral phosphite species in FeNKX-2. The peak in the region from 0 to –19.0 ppm can also be assigned to lower condensation degree of phosphorous species, which is in line with the IR spectroscopy data for FeNKX-2 samples proving the existence of P-H bond.[31,32] After 1 day of crystallization, the peak at –13.6 ppm is shifted to –14.6 ppm, and it is broadened as well. This is due to the distortion of the FeNKX-2 structure, in addition to the change of the chemical environment of P in the matrix during the ionothermal process. The small peak at –26.7 ppm is also observed which can be ascribed to P sites connected to both tetrahedral and octahedral Al sites, which are present in the AFI crystalline solid.[27] Thus, the NMR study reveals that phase transformation from FeNKX-2 to FeAPO-5 is taking place. The peaks shifting and broadening remain and the intensity of peak at –28.6 ppm, which corresponds to tetrahedral P species in the FeAPO-5, is increasing after 3 days. After 5 days of heating, a single peak at -29.3 ppm indicating the complete transformation to FeAPO-5 is detected.[22] As shown, the peak is sharp and this reveals that only one distinguishable type of tetrahedral phosphorus is present in the AFI structure.

Fe^{3+} substitution in the AlPO-5 framework can also be proven by ^{31}P MAS NMR spectroscopy besides observing the low field chemical shift of the peak of tetrahedrally coordinated Al in ^{27}Al MAS NMR spectrum (Fig. 5A(e)).[33-35] Due to the strong dipolar coupling

between ^{31}P and paramagnetic Fe^{3+} species, intense sidebands are usually observed in the MAS spectra. It can be seen that intense sidebands are observed even at the very early stage of ionothermal synthesis (Fig. 5). Thus, the ^{31}P MAS NMR spectroscopy data are in agreement with the UV-Vis spectroscopy, i.e. the Fe^{3+} participates actively in the crystallization process of FeAPO material.

^{13}C MAS NMR spectroscopy analysis

The $[bdmim]^+$ cations confined in the micropores of FeNKX-2 and FeAPO-5 samples was studied using ^{13}C MAS NMR spectroscopy. The results reveal that no carbon peaks are detected in the solid after 20 min of ionothermal heating, indicating that no $[bdmim]^+$ cation is confined in the micropores of the FeNKX-2 sample (Fig. 6a). Thus, it can be concluded that $[bdmim]^+$ cations do not play the role of a pore-filling agent during the formation of the FeNKX-2 framework structure. As the heating time was extended to 3 days, where the AFI phase started to form (Fig. 1), some small signals corresponding to $[bdmim]^+$ cation started to appear (Fig. 6b). The signals at 128.68 and 123.31 ppm are assigned to the C5 and C4 in the imidazole ring, and the resonance peaks at 36.65 and 9.41 ppm represent the C8 and C7 atoms of alkyl groups attached to the imidazole ring (inset of Fig. 6). Thus, ^{13}C NMR results imply that $[bdmim]^+$ cations start to be confined in the micropores of the FeAPO-5 sample, which is consistent with the IR results (inset of Fig. 4). The ^{13}C signals for $[bdmim]^+$ occluded in the AFI framework are becoming profound as the solid is further heated to 5 days, and fully crystalline FeAPO-5 is formed (Fig. 6c). As shown, all the signals are present thus indicating that the $[bdmim]^+$ molecules are preserved upon occlusion in the AFI crystals. Thus, the NMR spectroscopy data confirms that $[bdmim]^+$ cations act as a pore filling agent which directs the formation of FeAPO-5 during the ionothermal treatment.

Growth mechanism of FeAPO-5

Classically, AFI-type framework is templated by amines or quaternary ammonium salts under hydrothermal conditions using H_3PO_4 as a phosphorus source.[36] H_3PO_3 is generally described with the structural formula $HPO(OH)_2$ where this species exists in equilibrium with a $P(OH)_3$ tautomer. Because of the rapid interconversion, these tautomers alter the charge of P species in the NKX-2 and AFI frameworks ($P^{3+} \leftrightarrow P^{5+}$). Thus, the use of H_3PO_3 enables exploration of metastable intermediate phase with novel open-framework crystalline phase and unique framework properties. The use of H_3PO_3 as a phosphorus source, however, is seldom used in the synthesis of AlPO-*n* materials neither in hydrothermal[8,9,12] nor in ionothermal[17] pathways. On the other hand, it was reported that the dibasic H_3PO_3 acid (pKa_1 = 1.80, pKa_2 = 6.15) has stronger acidity compared to H_3PO_4 (pKa_1 = 2.12, pKa_2 = 7.21, pKa_3 = 12.67), and its acidity and oxidation state of P species also govern the selectivity of product crystalline phase during the crystallization process.[9,10]

The ionothermal synthesis pathway of FeAPO-5 *via* H_3PO_3-containing route is shown in Fig. 7. During the initial 10 min of heating, the process involves the mixing of raw aluminum isopropoxide, H_3PO_3 and $FeCl_3$ in the [bdmim]Cl ionic liquid, followed by successive dissolution (Stage I). As revealed by ^{27}Al MAS NMR, aluminum isopropoxide completely hydrolyzes within 10 min in polar [bdmim]Cl ionic liquid, and then further reacts with H_3PO_3 to form $Al(MO)_4(OH_2)_2$ (M = P, Fe) monomers and oligomers (Stage II). These intermediates are composed of H-P-O, P-O-Al, P-O-Fe and Al-O-Fe units where free phosphite and Fe^{3+} species are also present in the mixture.

In the absence of Fe^{3+}, the intermediates slowly undergo reorganization and NKX-2 structure is formed after 5 h of ionothermal heating or 6 days of hydrothermal treatment. The

crystallization rate, however, is significantly enhanced where the construction of NKX-2 framework structure is achieved merely in 20 min in the presence of Fe^{3+} under ionothermal heating (Stage III). During the crystallization process, Fe^{3+} species actively participate in the isomorphous incorporation in NKX-2 framework. After 20 min of ionothermal synthesis, 2.29 mol% of Fe has been incorporated in the framework of NKX-2. On the other hand, the Al species existed in FeNKX-2 are in the octahedral forms, and it is connected with HPO_3^{2-} tetrahedrals and AlO_6 octahedrals whereas the P species appears in the form of $P(H)(OAl_{Oct})_3$ tetrahedral species. No [bdmim]Cl is confined in the pores of FeNKX-2 as revealed by FTIR spectroscopy, indicating that $[bdmim]^+$ cation does not function as a pore filling agent during the construction of FeNKX-2 crystalline structure. As can be seen in the SEM image (Fig. 2b), the FeNKX-2 crystals (ca. 1.4-2.5 μm) exhibits a novel rounded rectangle-like morphology with rough surface.

After 1 day of ionothermal treatment, the FeNKX-2 crystals agglomerated with each other, forming big spherical particles (ca. 13.8 μm) (Stage IV). In addition, the peaks (1544, 1463 and 1425 cm^{-1}) corresponding to $[bdmim]^+$ appear in the IR spectrum of the solid sample (Fig. 4d). Thus, it indicates that the inorganic monomers and oligomers slowly enfold the $[bdmim]^+$ cations through van der Waals interactions to form AFI micropores.[27] This observation is supported by the XRD study where it reveals the beginning of phase transformation to AFI crystalline phase. During this period of time, the iron species in FeNKX-2 are gradually converted to tetrahedral framework iron species. Furthermore, the aluminum, which is octahedrally coordinated in the FeNKX-2, is partially converted into tetrahedrally coordinated Al in the AFI framework. The phosphorous is present in metaphosphite units where slightly distorted HPO_3^{2-} tetrahedral is slowly converted to PO_4^{3-} tetrahedral units *via* changing the oxidation state of P^{3+} to P^{5+}.

From the results we believe that transformation of pseudo-tetrahedral HPO_3^{2-} species (–7.7 kcal/mol) to tetrahedral PO_4^{3-} species (–12.0 kcal/mol) requires high activation energy.[37,38] That is the reason why no transformation of phosphorus species ($P^{3+} \rightarrow P^{5+}$) was observed in the absence of Fe^{3+}. However, the activation energy of transformation of pseudo-tetrahedral HPO_3^{2-} species to tetrahedral PO_4^{3-} species is significantly reduced with the addition of Fe^{3+}. The UV-Vis spectroscopy data reveals that Fe^{3+} initially exists in the form of ligand-to-metal charge transfer (LMCT) complex. This tetrahedral Fe^{3+} species can act as an intermediary electron-transfer medium allowing the change of oxidation state of P^{3+} to P^{5+}, and the tetrahedral Fe^{3+} species can even take part in the isomorphous incorporation in both the NKX-2 and AFI frameworks.

During FeAPO-5 nucleation process, the dissolved FeNKX-2 particles aggregate and form nuclei, which serve as the crystallization centre of FeAPO-5. Following the rapid nucleation process, the FeAPO-5 nuclei grow larger with time and form the AFI molecular sieve structure. The phase transformation continues to take place after 3 days (Stage V). This phenomenon can be proven based on the XRD study where the peaks corresponding to AFI phase are becoming dominant (Fig. 1c,d). Furthermore, the IR peak intensity of $[bdmim]^+$ is getting stronger (Fig. 4c,d) indicating that more and more $[bdmim]^+$ molecules are interacting and confined inside the micropores of FeAPO-5. The pseudo-tetrahedral HPO_3^{2-} species still co-exist with the tetrahedral PO_4^{3-} species in the FeNKX-2/FeAPO-5 intermediates. This transformation thus may lead to the highly strained tetrahedral T-atom sites present in the framework and act as the key role on the formation of FeAPO-5. Furthermore, the terminal P–H bond of HPO_3^{2-} slowly disappears with heating time *via* its tautomerism involving shifts of H between O and P.

After 5 days of heating, pure FeAPO-5 is formed. The size of crystals remain almost constant (ca. 14 μm) during the whole phase transformation process which can be explained by the slow and controlled oxidation-reduction chemistry reaction ($P^{3+} \rightarrow P^{5+}$) that favours the procedure for retarding the crystal growth of FeAPO-5 molecular sieves (Stage VI). At this stage, the structure of crystalline FeAPO-5 consists of an ordered covalent network involving tetrahedral $[PO_{4/2}]^+$, $[AlO_{4/2}]^-$ and $[FeO_{4/2}]^-$ units. Furthermore, the $[bdmim]^+$ is completely enfolded and occluded into the channels of FeAlPO-5 crystals based on FTIR spectroscopy data.[27]

4. Conclusions

A detailed investigation of the ionothermal synthesis of FeAPO-5 molecular sieve in the presence of H_3PO_3 has been reported. The results show that initially raw chemicals dissolve rapidly in [bdmim]Cl polar ionic liquid. By adding Fe^{3+} salt into the reaction mixture, FeNKX-2 intermediate is crystallized within 20 min instead of 3 h of heating. The study also reveals that $[bdmim]^+$ cation does not function as a pore-filling agent during the construction of FeNKX-2 crystalline structure. Phase transformation from FeNKX-2 to FeAPO-5 starts after 1 day of heating. During this stage, the tetrahedral Fe^{3+} species was found not only participating in the construction of the NKX-2/AFI framework but also acting as an intermediary electron-transfer medium. As a result, the oxidation of phosphite (P^{3+}) to phosphate (P^{5+}) was enhanced resulting in the fast release of phosphorus nutrient (P^{5+}) that are required for the crystallization and growing of FeAPO-5. Furthermore, confinement of $[bdmim]^+$ cations by anionic ferroaluminophosphate intermediate is also observed along the phase transformation process. Fully crystalline FeAPO-5 was obtained after 5 days of ionothermal synthesis.

Thus, the use of ionic liquids as dual solvents and templates in combination with H_3PO_3 as an alternative phosphorus source, offers the possibility of preparing the FeAPO microporous materials *via* phase transformation method. The highly porous FeAPO samples with insufficient thermal stability are not used in catalysis yet. However, considerable efforts in improving the thermal stability of the FeAPO samples for exploring further their catalytic properties are in progress.

Acknowledgments

The financial support from RUI (1001/PKIMIA/811264) and USM Short-term (304/PKIMIA/6313047) grants is acknowledged. J.P. Ghoy would also like to thank the MyBrain and USM fellowship for the scholarship provided.

References

1. S. Henninger, F. Schmidt and H.-M. Henning, *Applied Thermal Engineering*, 2010, **30**, 1692-1702.
2. E. P. Ng, L. Delmotte and S. Mintova, *ChemSusChem*, 2009, **2**, 255-260.
3. F. Adam, J.-T. Wong and E.-P. Ng, *Chemical Engineering Journal*, 2013, **214**, 63-67
4. E. Hu, Y. L. W. Huang, Q. Yan, D. Liu and Z. Lai, *Microporous and Mesoporous Materials*, 2009, **126**, 81-86.
5. E. Leite, T. Babeva, E.-P. Ng, V. Toal, S. MIntova and I. Naydenova, *The Journal of Physical Chemistry C*, 2010, **114**, 16767-16775.
6. M. K. Song and K. T. No, *international journal of hydrogen energy*, 2009, **34**, 2325-2328.
7. L. Tosheva, E.-P. Ng, S. Mintova, M. Holzl, T. H. Metzger and A. M. Doyle, *Chemistry of Materials*, 2008, **20**, 5721-5726.
8. N. Li, Y. Ma, S. Xiang and N. Guan, *Chemistry of materials*, 2006, **18**, 975-980.

9. W. Kong, W. Dai, N. Li, N. Guan and S. Xiang, *Journal of Molecular Catalysis A: Chemical*, 2009, **308**, 127-133.

10. P.W. Atkins, T. Overton, J.P. Rourke, M. Weller and F.A. Armstrong, *Inorganic Chemistry, Fifth ed.*, Oxford University Press, UK, 2010.

11. H. Chen, R. Chao, B. Na, N. Li, S. Xiang and N. Guan, *Chinese Journal of Catalysis*, 2007, **28**, 501-503.

12. N. Li, G. Cao and S. Xiang, *Studies in Surface Science and Catalysis*, 2004, **154**, 1001-1006.

13. E. R. Cooper, C. D. Andrews, P. S. Wheatley, P. B. Webb, P. Wormald and R. E. Morris, *Nature*, 2004, **430**, 1012-1016.

14. E. R. Parnham and R. E. Morris, *Accounts of chemical research*, 2007, **40**, 1005-1013.

15. T. Laher and C. Hussey, *Inorganic Chemistry*, 1983, **22**, 3247-3251.

16. E.-P. Ng, S. S. Sekhon and S. Mintova, *Chemical Communications*, 2009, 1661-1663.

17. Y. Shi, X. Zhang, L. Wang and G. Liu, *Materials Letters*, 2014, **124**, 212-214.

18. J. Kornatowski, G. Zadrozna, M. Rozwadowski, B. Zibrowius, F. Marlow and J. A. Lercher, *Chemistry of materials*, 2001, **13**, 4447-4456.

19. M. Dong, G. Wang, Z. Qin, J. Wang, T. Liu, S. Yuan and H. Jiao, *The Journal of Physical Chemistry A*, 2007, **111**, 1515-1522.

20. L. Qi, X. Qi, J. Wang and L. Zheng, *Catalysis Communications*, 2011, **16**, 225-228.

21. F. Wang, L. Liang, J. Ma and J. Sun, *Materials Letters*, 2013, **111**, 201-203.

22. D. Y. Khoo, W.-M. Kok, R. R. Mukti, S. Mintova and E.-P. Ng, *Solid State Sciences*, 2013, **25**, 63-69.

23. A. Bruckner, U. Lohse and H. Mehner, *Microporous and mesoporous materials*, 1998, **20**, 207-215.

24. W. Wei, J. A. Moulijn and G. Mul, *Microporous and Mesoporous Materials*, 2008, **112**, 193-201.

25. A. Kostapapas, S.L. Suib, R.W. Coughlin and M.L. Occelli, in *P.A. Jacobs, R.A. van Santen (Eds.), Zeolites: Facts, Figures, Future: Facts, Figures, Future*, Elsevier Science Publishing Company Inc., Netherlands, 1990, pp. 399-409.

26. D. Y. Khoo, H. Awala, S. Mintova and E.-P. Ng, *Microporous and Mesoporous Materials*, 2014, **194**, 200-207.

27. E. P. Ng, L. Itani, S. S. Sekhon and S. Mintova, *Chemistry-A European Journal*, 2010, **16**, 12890-12897.

28. N. Y. Turova, V. Kozunov, A. Yanovskii, N. Bokii, Y. T. Struchkov and B. Tarnopol'skii, *Journal of Inorganic and Nuclear Chemistry*, 1979, **41**, 5-11.

29. K. Folting, W. E. Streib, K. G. Caulton, O. Poncelet and L. G. Hubert-Pfalzgraf, *Polyhedron*, 1991, **10**, 1639-1646.

30. R. D. Gougeon, E. B. Brouwer, P. R. Bodart, L. Delmotte, C. Marichal, J.-M. Chézeau and R. K. Harris, *The Journal of Physical Chemistry B*, 2001, **105**, 12249-12256.

31. A. Sayari, I. Moudrakovski, J. S. Reddy, C. I. Ratcliffe, J. A. Ripmeester and K. F. Preston, *Chemistry of materials*, 1996, **8**, 2080-2088.

32. Z. Luan, D. Zhao, H. He, J. Klinowski and L. Kevan, *The Journal of Physical Chemistry B*, 1998, **102**, 1250-1259.

33. B. Chen and Y. Huang, *Microporous and Mesoporous Materials*, 2009, **123**, 71-77.

34. C. Montes, M. E. Davis, B. Murray and M. Narayana, *Journal of Physical Chemistry*, 1990, **94**, 6425-6430.

35. S.-H. Chen, S.-P. Sheu and K.-J. Chao, *J. Chem. Soc., Chem. Commun.*, 1992, 1504-1505.

36. R. Szostak, in *Synthesis*, Springer, 1998, pp. 157-185.

37. W.-Y. Tsang, T. L. Amyes and J. P. Richard, *Biochemistry*, 2008, **47**, 4575-4582.

38. A. C. Reyes, X. Zhai, K. T. Morgan, C. J. Reinhardt, T. L. Amyes and J. P. Richard, *Journal of the American Chemical Society*, 2015, **137**, 1372-1382.

Figure captions

Fig. 1 XRD patterns of solid products after (a) 10 min, (b) 20 min, (c) 1 day, (d) 3 days and (e) 5 days of ionothermal synthesis. The XRD pattern of pure NKX-2 aluminophosphite is shown in (f).

Fig. 2 SEM images of solid products after (a,b) 10 min, (c,d) 20 min, (e,f) 1 day, (g,h) 3 days and (i,j) 5 days of ionothermal synthesis at different magnifications.

Fig. 3 UV-visible spectra of solid products after (a) 10 min, (b) 20 min, (c) 1 day, (d) 3 days and (e) 5 days of ionothermal synthesis.

Fig. 4 IR spectra of solid products after (a) 10 min, (b) 20 min, (c) 1 day, (d) 3 days and (e) 5 days of ionothermal synthesis.

Fig. 5 (A) ^{27}Al and (B) ^{31}P MAS NMR spectra of solid products after (a) 10 min, (b) 20 min, (c) 1 day, (d) 3 days and (e) 5 days of ionothermal synthesis.

Fig. 6 ^{13}C MAS NMR IR spectra of solid products after (a) 10 min, (b) 3 days and (c) 5 days of ionothermal synthesis.

Fig. 7 The ionothermal crystallization pathway of FeAPO-5 from H_3PO_3-containing route.

Figures

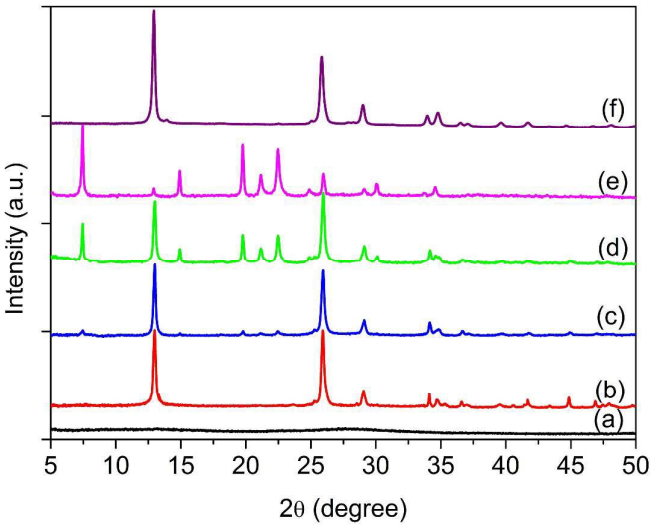

Fig. 1

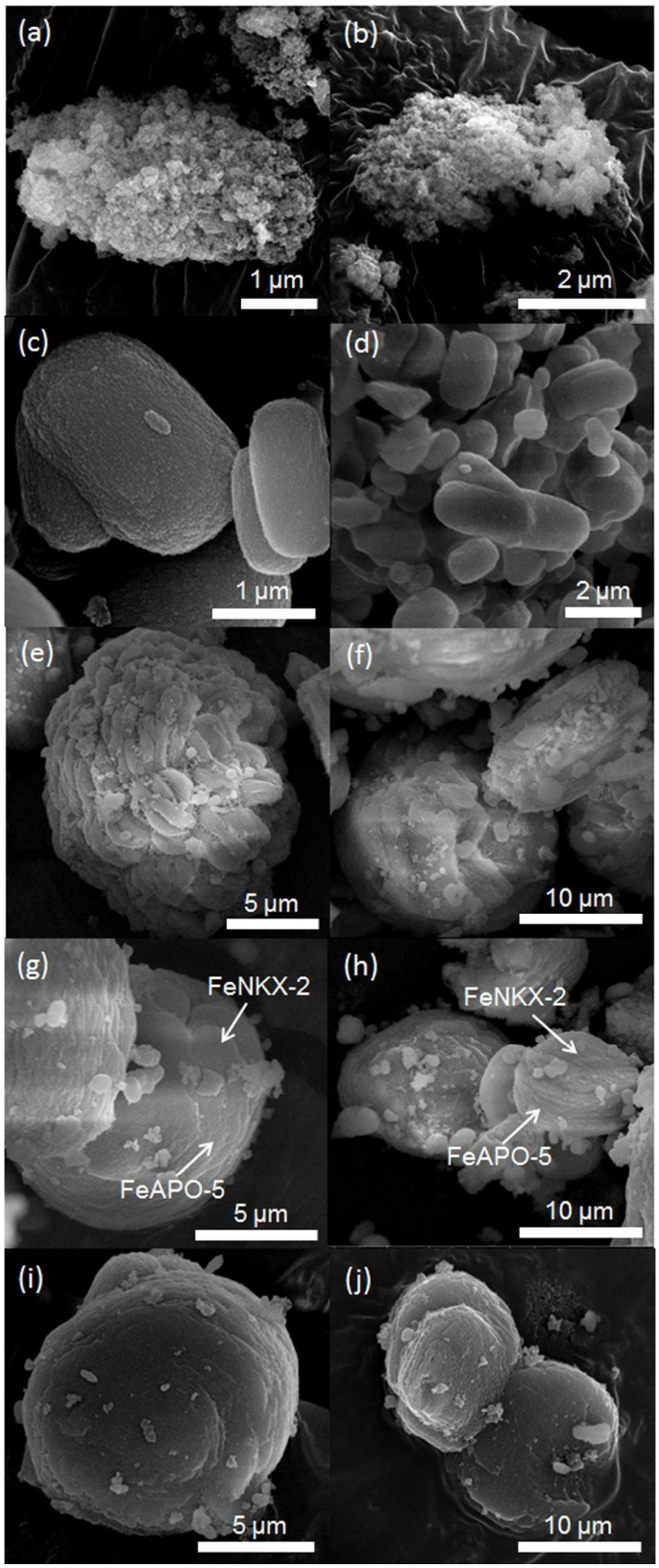

Fig. 2

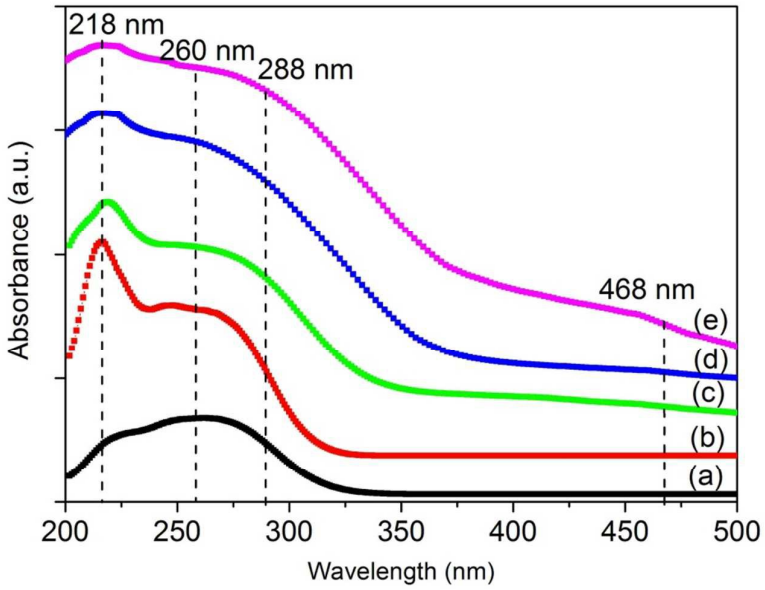

Fig. 3

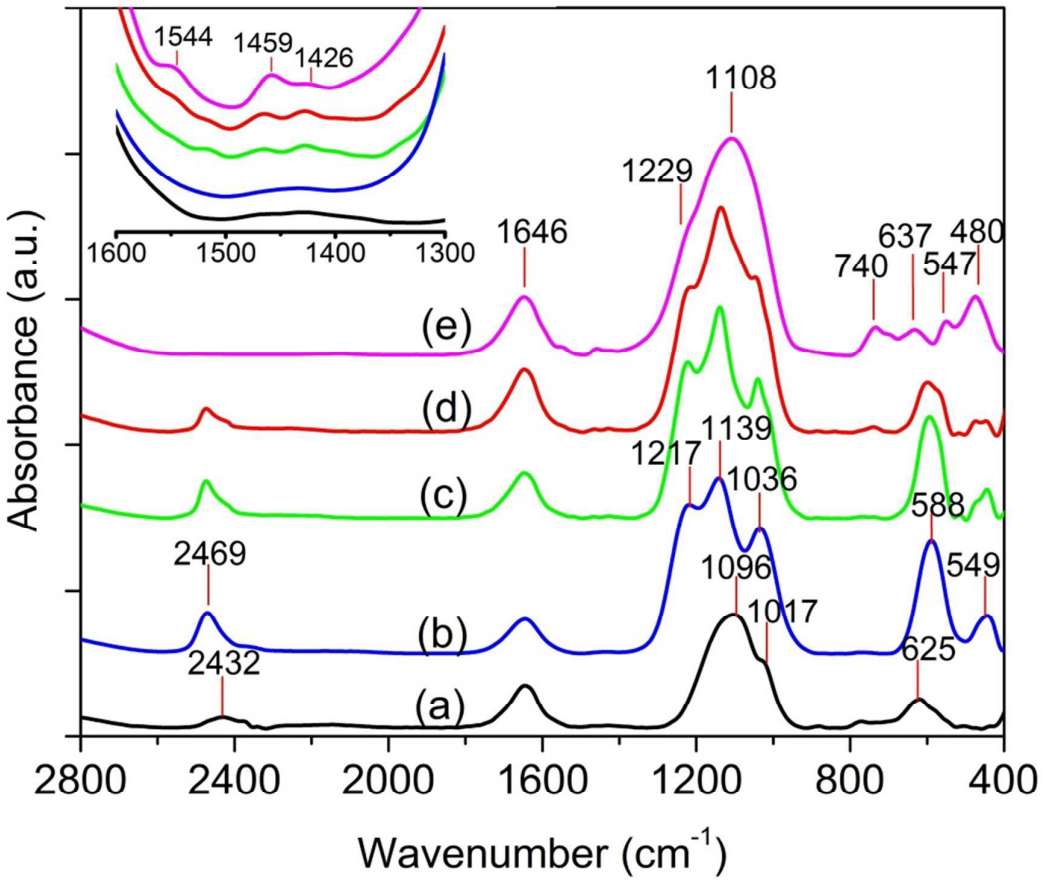

Fig. 4

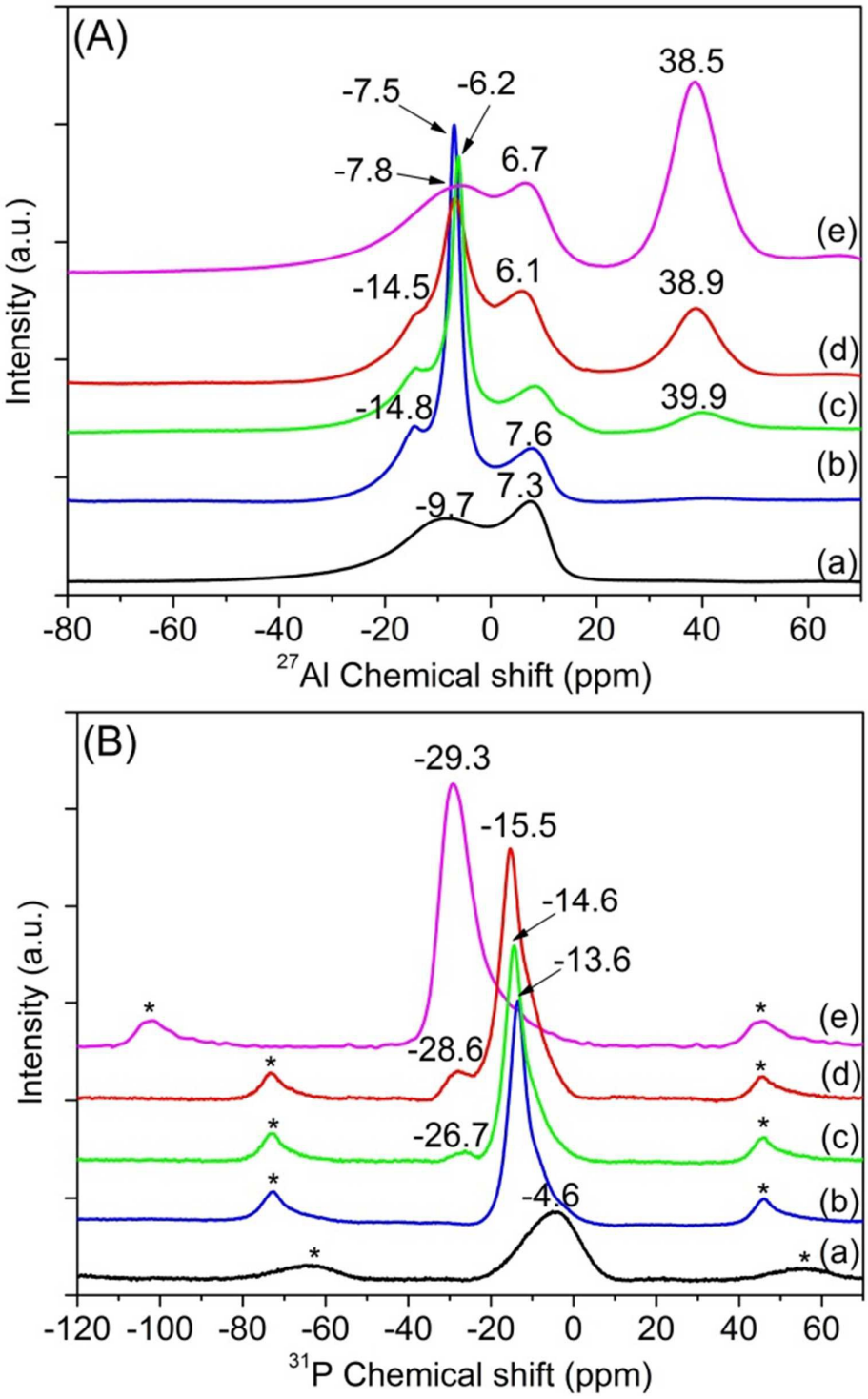

Fig. 5

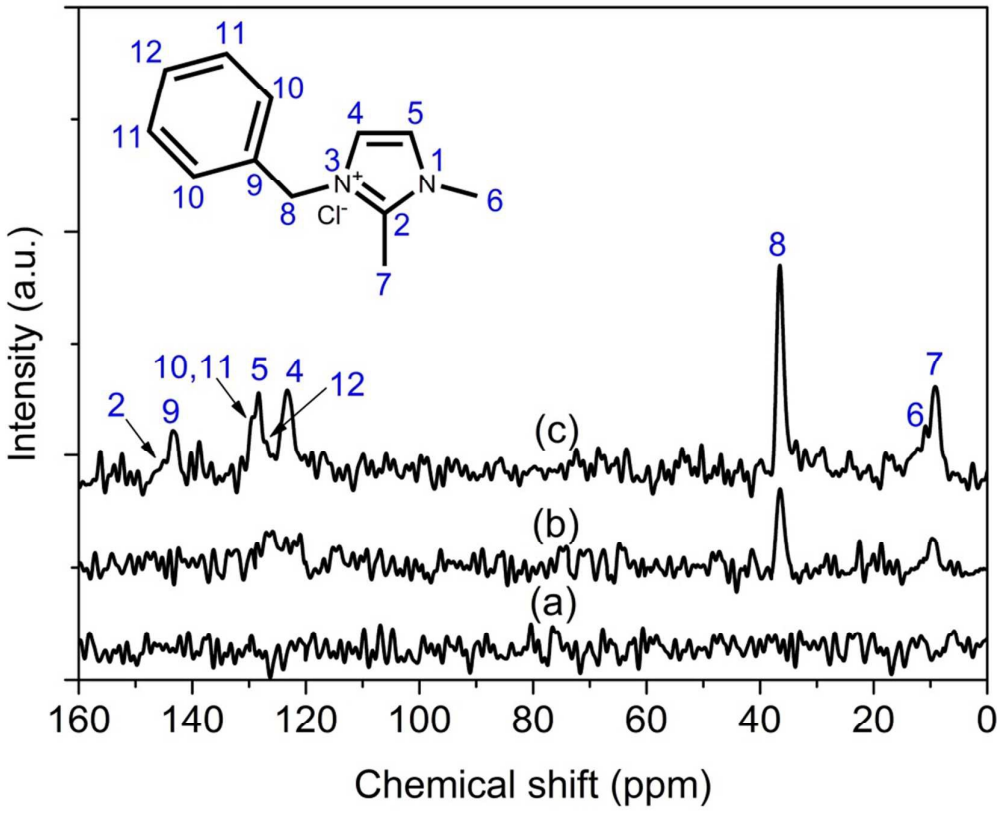

Fig. 6

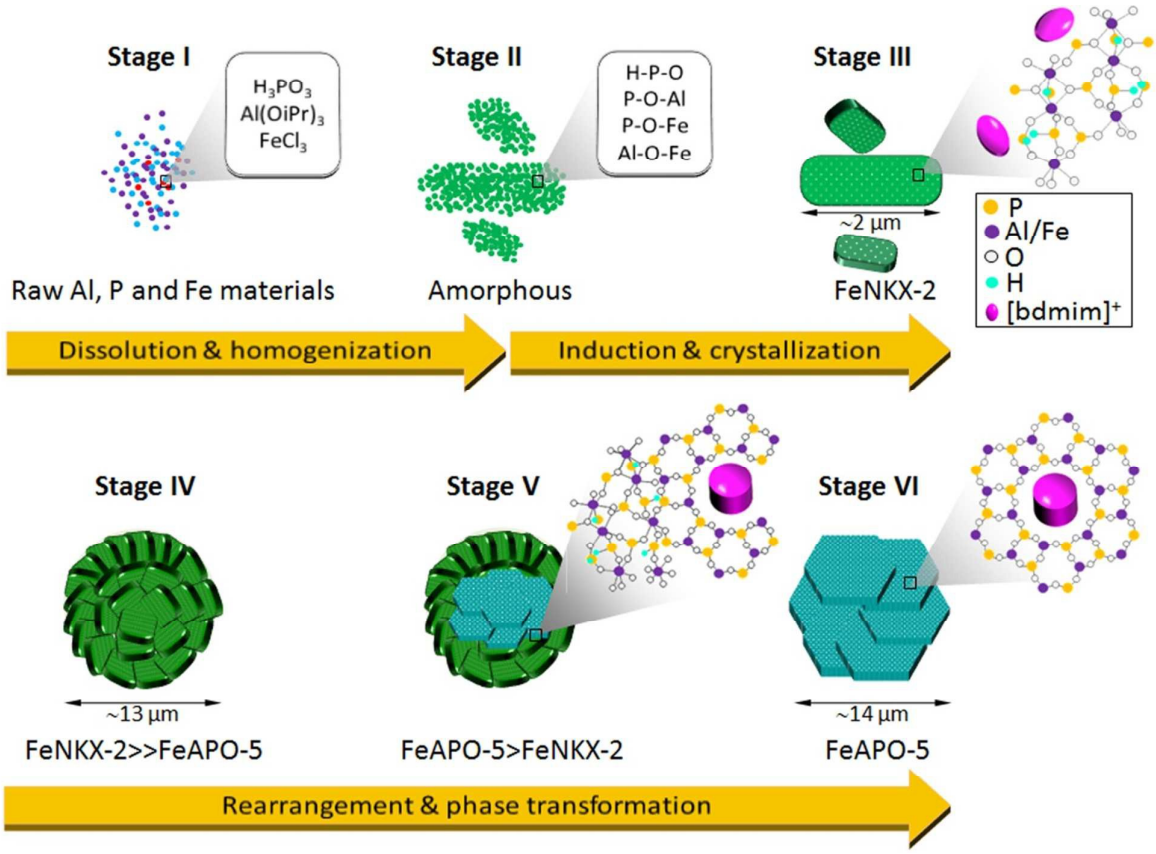

Fig. 7

Table

Table 1 Framework compositions of the solid samples.

Phase(s)	Crystallization time	Atomic ratios			P/(Al+Fe) ratio	Fe/(Al+P+Fe) ratio (mol%)
		Al	P	Fe		
Amorphous	10 min	0.611	1.000	0.025	1.57	1.53
FeNKX-2	20 min	0.619	1.000	0.038	1.52	2.29
FeNKX-2, FeAPO-5*	1 day	0.670	1.000	0.051	1.39	2.96
FeNKX-2, FeAPO-5	3 days	0.826	1.000	0.061	1.13	3.23
FeAPO-5	5 days	0.938	1.000	0.068	0.99	3.39

*Trace amount

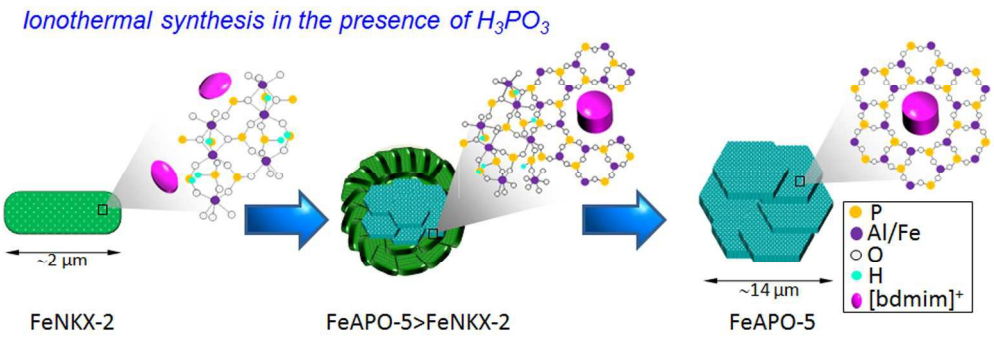

340x120mm (300 x 300 DPI)